Eur. Phys. J. D **39**, 331–350 (2006)
DOI: 10.1140/epjd/e2006-00121-4

THE EUROPEAN PHYSICAL JOURNAL D

The Ne II spectrum*

A.E. Kramida[a] and G. Nave

National Institute of Standards and Technology, Gaithersburg, MD 20899, USA

Received 29 November 2005 / Received in final form 27 February 2006
Published online 7 June 2006 –

Abstract. Spectra of neon-filled hollow cathode discharge lamps were observed by means of high-resolution Fourier-transform spectroscopy (FTS) covering the region from vacuum ultraviolet to near infrared. By combining these new measurements with results of other FTS and grating spectroscopy observations, we compiled a complete list of approximately 1700 spectral lines of Ne II covering the range from 324 Å to 130000 Å. All known energy levels of Ne II were derived from this line list with improved accuracy. The newly optimized energy levels were used to derive a set of Ritz wavelength standards in the vacuum ultraviolet that are in good agreement with the previously used data. An improved classification of energy levels was made with the help of parametric calculations, and the existing controversy in the naming of strongly mixed levels was resolved.

PACS. 32.10.Fn Fine and hyperfine structure – 32.30.Jc Visible and ultraviolet spectra – 32.30.Bv Radio-frequency, microwave, and infrared spectra – 31.15.Ct Semi-empirical and empirical calculations (differential overlap, Huckel, PPP methods, etc.) – 95.30.Ky Atomic and molecular data, spectra, and spectral parameters (opacities, rotation constants, line identification, oscillator strengths, gf values, transition probabilities, etc.)

1 Introduction

The most extensive analysis of the Ne II spectrum was done by Persson in 1971 [1]. The history of prior studies of this spectrum can be found therein. Persson's analysis covered the wavelength region 324 Å to 11000 Å and provided a set of reference wavelengths in the 300 Å to 460 Å and 1000 Å to 2000 Å regions. These reference wavelengths are widely used by spectroscopists, since the Ne II spectrum is easy to excite, and, as noted by Persson, "no neutral and only a very limited number of singly ionized atoms, among them neon, have emission lines of reasonable intensities below 460 Å" [1]. Persson used three spectrographs equipped with different diffraction gratings to photograph different regions of the spectrum. His experimental equipment permitted him to achieve the best spectral resolution available with grating spectroscopy. Since then, the technique of Fourier transform spectroscopy (FTS) became a popular means of obtaining precision spectral data. In a number of FTS studies of various spectra, neon-filled hollow cathode discharges were used to produce the needed spectrum. However, neon itself was never the immediate subject of these studies, except for one work by Sansonetti et al. [2] devoted exclusively to Ne I. The other experiments were devoted to the spectra of thorium (Palmer and Engleman [3]), magnesium (Biémont and Brault [4] and Quinet et al. [5]), vanadium (Quinet et al. [5]), and iron (Nave et al. [6]). As a by-product, they produced sets of precisely measured wavelengths of neutral and ionized neon.

The infrared lines of Ne II observed by Biémont and Brault [4] were published by Quinet et al. [5] along with a set of new energy levels derived from them. However, the new levels found by Quinet et al. [5] were based on Persson's list of energy levels [1], in which relative uncertainties of the levels are much greater than the uncertainties of wave numbers measured by Quinet et al. The relative uncertainties of levels given by Persson [1] are typically about a few hundredth of cm^{-1} [1], while the measurement uncertainties of wave numbers obtained by Quinet et al. [5]) were lower by a factor of ten. As a consequence, the level values proposed by Quinet et al. [5] are not precisely consistent with the wave numbers given therein. This presents a problem, for example, in the modeling of infrared spectra of terrestrial and celestial sources.

* The full version of Table 1 is only available in electronic form at `http://www.eurphysj.org`.

[a] e-mail: `Alexander.Kramida@nist.gov`

[1] The customary unit cm^{-1} for energy levels, used here, is related to the SI unit for energy (joule) by 1 cm^{-1} = 1.986 445 61(34) × 10^{-23} J [P.J. Mohr, B.N. Taylor, Rev. Mod. Phys. **77**, 1 (2005)].

The positions of predicted lines would not coincide with the observed ones.

The neon lines observed by Palmer and Engleman [3] were given in their thorium atlas without classification. This makes it difficult to identify them with transitions in Ne I and II. In addition, this publication is not easily accessible. Some of the Ne II wavelengths given by Palmer and Engleman [3] were reproduced in the atlas of the spectrum of a Pt/Ne lamp [7], which is available on the World Wide Web. However, the lines cited there from Palmer and Engleman [3] are also given without classification. The wavelength uncertainty specified there for these Ne II lines was given as ±0.0001 Å, or 0.0011 cm^{-1} at 3000 Å. This appears too optimistic compared with the uncertainty of ±0.003 cm^{-1} quoted in Palmer and Engleman [3] for Ne lines without a distinction between the strong and weak lines. For the latter, the uncertainty would be expected to be much greater. In a recent compilation of Ne I lines by Saloman and Sansonetti [8], the uncertainties of strong Ne I lines from Palmer and Engleman [3] were estimated as ±0.003 cm^{-1}, while the uncertainties of the weakest lines were given as ±0.015 cm^{-1} with an average of ±0.009 cm^{-1}. We have discussed the derivation of the Ne II uncertainties with one of the authors of reference [7] (C. Sansonetti), and he agreed that the uncertainties of the Ne II wavelengths quoted from Palmer and Engleman [3] should be increased by a factor of 3 for the strong lines, and more for weak lines.

The neon lines measured in the spectra of Fe/Ne hollow cathodes by Nave et al. [6] were not published previously. These measurements are particularly valuable because they extend to the vacuum ultraviolet (VUV) region.

It seems very promising to replace Persson's wavelengths with more precise FTS ones and obtain an improved set of energy levels. This could improve the accuracy of the reference wavelengths in the VUV region, which, as noted above, are widely used in modern spectroscopy.

In addition to these experimental problems, there exists a long-standing controversy in the physical interpretation of some of the levels. Although Persson provided a very convincing interpretation of most levels [1], he indicated that some of the $2p^4(^3P)3d$ levels have ambiguous designations. He mentioned that Luyken [9] proposed another description of these levels based on his intermediate coupling calculations, but these calculations do not provide a good proof of the proposed changes. However, recent calculations of Tachiev and Froese Fischer [10] provide further support to Luyken's interpretation. As noted by Persson [1], classification of the 4*d*, 5*d*, and 6*d* levels was done similar to the 3*d* configuration. Thus, it is likely that the changes in classification of the 3*d* levels should also be followed by similar changes in the other *nd* configurations.

The goals of the present paper were to compile the most complete list of precisely measured lines of Ne II, derive an improved set of energy levels that would be consistent with all observed wavelengths, and provide a corrected interpretation of the energy levels.

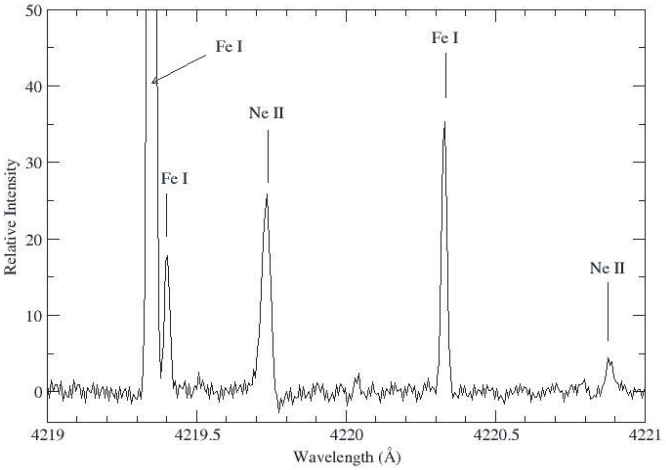

Fig. 1. A portion of a spectrum of an iron-neon hollow cathode lamp. 21 scans were taken with roughly 500 Pa of neon at a current of 750 mA.

2 New FTS measurements

The Fourier-transform (FT) spectra used in the present investigation were the same as those used in the studies of the Fe II spectrum by Nave et al. [6]. The source was a hollow cathode discharge lamp with an iron cathode operated with different pressures of neon. The spectra in the VUV and ultraviolet (UV) regions were taken with 260 Pa to 400 Pa (2 to 3 Torr) of neon and a current of 350 mA to 450 mA. The spectra in the visible and near infrared (IR) regions were taken with roughly 500 Pa (4 Torr) of neon and a current of 750 mA to 1 A. Relative line widths for Ne II (dominated by Doppler broadening) were $\Delta\lambda/\lambda = 7 \times 10^{-6}$ for the VUV and UV regions and 8×10^{-6} for the visible and near IR regions. The measurement procedures and other experimental details were described in Nave et al. [6] and in our recent paper on Ne III [11].

The Fe II wave-number measurements in Nave et al. [6] were calibrated with respect to 26 Ar II lines between 4300 Å and 5160 Å. The wave numbers for these lines were taken from Norlén [12], who used Fabry-Perot interferometry to measure them with respect to standard lines in ^{86}Kr. The Ar II lines used have since been remeasured by Whaling et al. [13] using Fourier transform spectroscopy with molecular CO lines as wave-number standards. The wave numbers of Whaling et al. are systematically higher than those of Norlén by 6.7 parts in 10^8. Since Whaling's wave numbers are of higher accuracy than those of Norlén, we have increased the wave numbers of Ne II lines measured in the Fe/Ne spectra by a factor of $6.7 \times 10^{-8}\sigma$ to bring them on the scale of Whaling et al. [13].

A portion of a spectrum containing some lines of Ne II is presented in Figure 1. The neon lines usually had a

noticeable asymmetry caused by the presence of approximately 9% of the ^{22}Ne isotope in the natural neon gas that consists primarily of ^{20}Ne.

In addition to the asymmetry, the neon lines could usually be distinguished from the iron lines by their width being greater than the width of the iron lines by a factor of approximately 1.7. However, both the larger width and asymmetry can be caused not only by the difference in Doppler broadening, but also by blending of two or more lines. Thus, we excluded from our list of Ne II lines those lines identified in the Fourier-transform (FT) spectra that could possibly be blended with lines of Fe I or Fe II. Such possible blends were identified by the existence of an allowed dipole transition between two opposite-parity levels of Fe I or Fe II [14] with a wavelength within the half-width of the measured Ne II line.

For symmetric lines, the presence of self-absorption should not affect the centroid of the line. However, for asymmetric lines (e.g. Ne II lines affected by isotopic structure), self-absorption may preferentially absorb the strongest component, thus shifting the centroid of the line toward the weaker component. This can be checked by fitting two components to lines that may be self-absorbed and that may have isotopic structure. We decomposed several profiles of strong isolated Ne II lines into pairs of peaks. The difference of the wave numbers obtained for the strongest peak in each of the decomposed profiles from the values obtained by fitting the profile with a single peak was always much smaller than the measurement uncertainty. This indicates that the effects of self-absorption, combined with the isotopic asymmetry of the line profiles, do not significantly shift the measured positions of the lines in our spectra. Such effects should also be negligible for the grazing-incidence spectra taken by Persson [1] at very low neon pressures. For other spectra used in this work, we could only estimate the significance of self-absorption effects by comparing the relative intensities of the strongest lines with those observed in our spectra, as well as with the radiative rates calculated by means of parametric fitting. These comparisons do not indicate presence of strong self-absorption in the used spectra.

3 Analysis of possible Stark shifts

Stark shifts and pressure shifts might affect the wave numbers of the lines in our spectra and in the other studies used in this compilation. In order to check for these shifts, we compared the wave numbers in our Fe/Ne spectra measured with different pressures of neon. In addition, we compared wave numbers measured in our Fe/Ne spectra with FTS measurements made by Palmer and Engleman [3] using a commercial sealed Th/Ne hollow cathode lamp, and also compared the wave numbers measured by Palmer and Engleman [3] with the measurements of Quinet et al. [5]. The results of these comparisons are presented in Figure 2. Panel a shows the differences in wave numbers between two of our FT spectra: one taken at medium neon pressures (260 Pa to 400 Pa), and the other taken at low (roughly 70 Pa) neon pressure. Panel (b) shows the differences in wave numbers between the Th/Ne spectrum [3] with roughly 700 Pa of Ne at 75 mA and our Fe/Ne spectrum taken with roughly 500 Pa of neon at a current of 750 mA. Panel (c) shows the differences in wave numbers between the Th/Ne spectrum [3] and Mg/Ne spectrum [5] taken with approximately 100 Pa of neon. The differences in wave numbers are plotted in Figure 2 vs. the energy of the upper level of the transition.

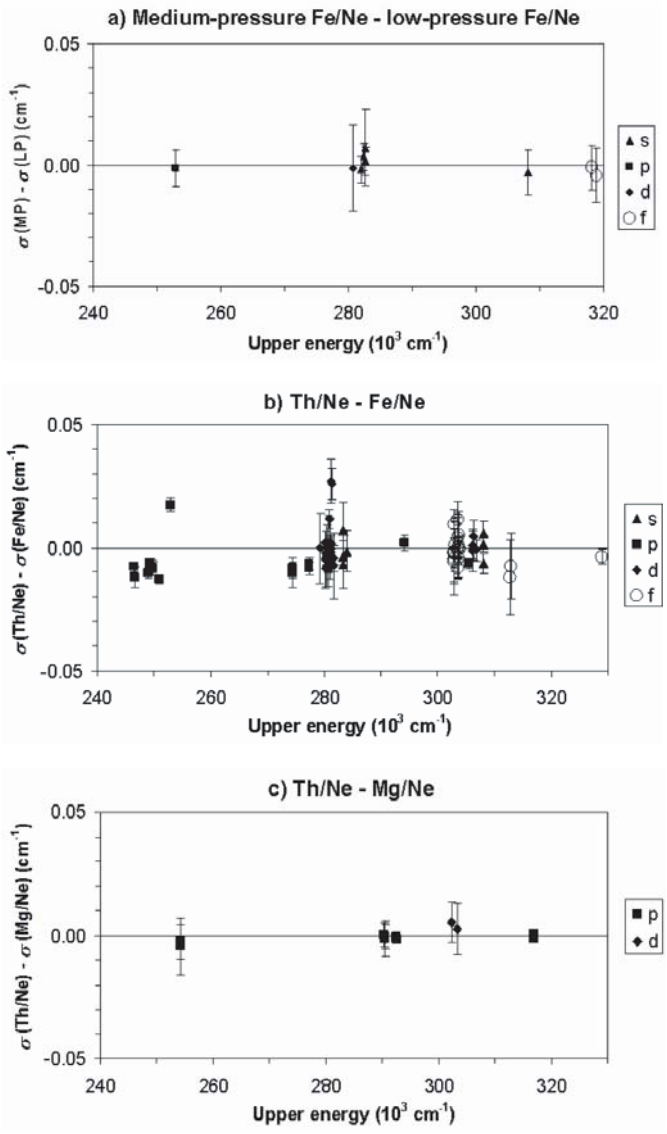

Fig. 2. Wave-number differences between Ne II lines measured in different spectra. (a) Differences in wave numbers between the lines measured in our medium- and low-pressure Fe/Ne spectra; (b) differences in wave numbers between the lines measured in the Th/Ne spectrum by Palmer and Engleman [3] and in our high-pressure Fe/Ne spectrum; (c) differences in wave numbers between the Th/Ne spectrum [3] and the Mg/Ne spectrum measured by Quinet et al. [5]. The legends describe the orbital momentum of the outer electron for the upper energy level of a transition: (▲) *s* shell, (■) *p* shell, (♦) *d* shell, and (○) *f* shell. The error bars represent the measurement uncertainties (one standard deviation).

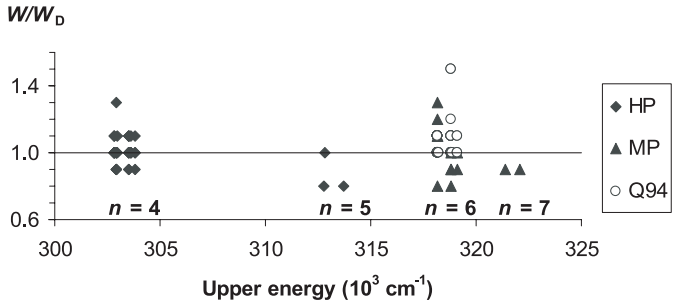

Fig. 3. Ratios of the observed line width W to the Doppler width W_D for the lines originating from the nf and ng levels of Ne II. The legends describe the different spectra where these lines were observed: HP – our Fe/Ne spectrum taken with 500 Pa of neon at a current of 750 mA (♦), MP – our Fe/Ne spectrum taken with 260 to 400 Pa of neon at a current of 350 mA (▲), Q94 – Mg/Ne/Ar spectrum [5] taken at 100 Pa of neon and 1.6 Pa of argon (○).

If the Stark shifts were present in the used light sources, they would be the largest for the lines with the highest upper energy and angular momentum. This would result in increased scatter of wave-number differences for higher excitation energies. Figure 2 shows that there is no such trend in the spectra used in this work.

Furthermore, if Stark shifts were present, they would be accompanied by a noticeable broadening of lines originating from levels with high angular momentum. The well-known physical processes that may cause Stark shifts in the hollow cathode discharge are collisions with electrons, ions, and neutral atoms. Besides the line shifts, these processes would also lead to line broadening. This is also true for the Stark shifts caused by a static electric field penetrating into the glow region. Such shifts were observed by Zhechev and Parvanova [15] in a hollow cathode discharge with a very special geometry (short and wide, as opposed to the long and narrow cathodes used for spectroscopic studies). It was demonstrated that the Stark shifts caused by this effect strongly vary with the distance of an emitting region from the cathode. Thus, in space-integrated spectra like ours or those reported by Palmer and Engleman [3] and Quinet et al. [5] these varying shifts would cause line broadening. The Stark broadening should be the largest for the lines originating from the levels with the highest principal quantum number, as the level separations become smaller. Figure 3 shows the ratios of the observed line width W to the Doppler width W_D for the lines originating from the nf and ng levels in our Fe/Ne spectra and in the Mg/Ne spectrum measured by Quinet et al. [5]. As seen from Figure 3, there is no systematic trend of increasing the line width with increasing principal quantum number of the upper level. The observed deviations of W/W_D from unity in most cases can be explained by measurement uncertainties (see Sect. 5).

Persson [1] also noted that even the highest observed members of the $4f - ng$ series showed no noticeable broadening in his Ne II spectra obtained with a hollow cathode lamp operated at very low pressures (7 to 11 Pa).

Thus, we conclude that none of the spectra used in the present work possess Stark or pressure shifts that exceed the wavelength-measurement uncertainty. This finding is in contrast to the results of Chang et al. [16] for Ne I. They investigated the Stark shifts of the lines of neutral neon observed in the same spectra that were used by Quinet et al. [5] and found that the $6f$, $6g$, and $7g$ levels of Ne I were shifted by as much as 0.035 cm^{-1}.

It is seen from Figure 2b that some of the lines originating from low-lying p-shell levels exhibit rather large wave-number differences between the Th/Ne and Fe/Ne spectra, which are well outside of the measurement uncertainties. As argued above, these differences cannot be attributed to the Stark effect. The possible causes of these differences are blending with unidentified metal lines and strong self-absorption. Although we checked that self-absorption does not significantly shift the centroids of the Ne II lines in our FTS spectra (see Sect. 2), such shifts cannot be totally excluded for the other spectra used in this work, such as the FTS spectrum of Palmer and Engleman [3]. In the cases where we observed large wave-number differences between different spectra, we selected the measurements that are in better agreement with the other observed combinations in the Ne II spectrum and discarded the deviating observations.

4 Observed lines of Ne II

The compiled list of observed lines of Ne II is presented in Table 1. Out of the total 1623 measured wavelengths, 920 are due to Persson [1].

Wavelengths of 331 lines from Persson's list [1] were precisely measured using FTS in one or more spectra of various hollow cathode discharges (in Palmer and Engleman [3] and in the present work). We excluded from the list of neon lines given by Palmer and Engleman [3] those lines that could possibly be blended with thorium lines. Similarly to the procedure that was used for the Fe/Ne spectrum (see Sect. 2), such possible blends were identified by the existence of an allowed dipole transition between two opposite-parity levels of Th I or Th II [17] with a wavelength within the half of the full width at half maximum (FWHM) of the measured Ne II line.

The line at 2693.3555 Å deserves special attention because this is the only line observed in the FTS spectra that connects the first excited configuration, $2s2p^6$, with the upper levels. The other lines terminating at the $2s2p^6\,{}^2\mathrm{S}_{1/2}$ level are either too weak or have too short wavelength. Thus, the accuracy of the position of almost all excited levels strongly depends on the measurement accuracy of this line. Persson [1] observed this line at 2693.356 ± 0.003 Å. In our Fe/Ne spectra, this line was observed at 2693.3557 ± 0.0008 Å. However, it was broad and asymmetric, which indicated possible blending with an iron line. Thus, one of the present authors (Nave) has measured this line on three FT spectrograms taken with Pt/Cr/Ne and Cr/Ne sealed hollow cathode lamps. These spectrograms had a high signal-to-noise ratio and were

Table 1. Observed and predicted lines of Ne II (the full version of Table 1 is available in the *Supplementary Online Material*).

λ_{obs} (Å)[a]	$\delta\lambda^{b}_{obs}$ (Å)	σ_{obs} (cm^{-1})	Obs. intensity[c]	λ_{Ritz} (Å)	$\delta\lambda^{d}_{obs}$ (Å)	Transition[e]	$\Delta\lambda^{f}_{obs}$ (Å)	Ref[g]
...								
1826.667	0.005	54744.52	12	1826.66072	0.00008	$(^3P)3p\ ^4D^\circ_{3/2} - (^3P)5s\ ^2P_{1/2}$	0.006	P71
1826.829	0.005	54739.66	180	1826.8328	0.0011	$(^1D)3p\ ^2F^\circ_{7/2} - (^1D)5s\ ^2D_{5/2}$	–0.004	P71
1831.481	0.005	54600.62	22	1831.48203	0.00009	$(^3P)3p\ ^4D^\circ_{1/2} - (^3P)5s\ ^2P_{1/2}$	–0.001	P71
1833.9102	0.0014	54528.30	160	1833.91010	0.00008	$(^3P)3p\ ^4D^\circ_{5/2} - (^3P)5s\ ^2P_{3/2}$	0.0001	MP
1842.341	0.005	54278.77	140	1842.34135	0.00008	$(^3P)3p\ ^4D^\circ_{3/2} - (^3P)5s\ ^2P_{3/2}$	0.000	P71
1843.908	0.005	54232.64	160	1843.91039	0.00009	$(^3P)3p\ ^4D^\circ_{3/2} - (^3P)5s\ ^4P_{1/2}$	–0.002	P71
1845.9963	0.0010	54171.29	160	1845.99670	0.00008	$(^3P)3p\ ^4D^\circ_{7/2} - (^3P)5s\ ^4P_{5/2}$	–0.0004	MP
1847.249	0.005	54134.55	12	1847.24590	0.00009	$(^3P)3p\ ^4D^\circ_{1/2} - (^3P)5s\ ^2P_{3/2}$	0.003	P71
1848.8243	0.0013	54088.43	140	1848.82331	0.00009	$(^3P)3p\ ^4D^\circ_{1/2} - (^3P)5s\ ^4P_{1/2}$	0.0010	MP
1849.381	0.005	54072.15	180	1849.37844	0.00008	$(^3P)3p\ ^4D^\circ_{5/2} - (^3P)5s\ ^4P_{3/2}$	0.003	P71
1853.1166	0.0016	53963.15	180	1853.11518	0.00008	$(^3P)3p\ ^4D^\circ_{7/2} - (^3P)4d\ ^4P_{5/2}$	0.0014	MP
1853.453	0.005	53953.35	40	1853.4523	0.0011	$(^1D)3p\ ^2F^\circ_{5/2} - (^1D)4d\ ^2F_{5/2}$	0.001	P71
1854.0396	0.0006	53936.281	180	1854.02797	0.00007	$(^3P)3p\ ^2P^\circ_{3/2} - (^1D)4s\ ^2D_{3/2}$	0.0116	MP
				1854.04037	0.00007	$(^3P)3p\ ^2P^\circ_{3/2} - (^1D)4s\ ^2D_{5/2}$	–0.0008	MP
1854.976	0.005	53909.05	40	1854.9769	0.0010	$(^1D)3p\ ^2F^\circ_{7/2} - (^1D)4d\ ^2F_{7/2}$	–0.001	P71
1857.565	0.005	53833.92	60	1857.56461	0.00008	$(^3P)3p\ ^4D^\circ_{5/2} - (^3P)5s\ ^4P_{5/2}$	0.000	P71
1857.952	0.005	53822.70	140	1857.95285	0.00009	$(^3P)3p\ ^4D^\circ_{3/2} - (^3P)5s\ ^4P_{3/2}$	–0.001	P71
1858.4093	0.0010	53809.46	160	1858.41000	0.00007	$(^3P)3p\ ^2P^\circ_{1/2} - (^1D)4s\ ^2D_{3/2}$	–0.0007	MP
1859.017	0.005	53791.87	40	1859.01487	0.00009	$(^3P)3p\ ^4D^\circ_{5/2} - (^3P)4d\ ^2P_{3/2}$	0.002	P71
1859.361	0.005	53781.92	160	1859.36081	0.00008	$(^3P)3p\ ^4D^\circ_{7/2} - (^3P)4d\ ^2F_{5/2}$	0.000	P71
...								

[a]Observed and Ritz wavelengths are given in vacuum for lines shorter than 2000 Å and longer than 60000 Å. For the rest of the lines, the wavelengths are given in standard air. Conversion from vacuum to air was done using the five-parameter formula for the index of refraction of air from Peck and Reeder [21]. The wave numbers of the lines cited from Boyce [18] and Persson [1] are derived from the wavelengths; in the air region, the same formula of Peck and Reeder [21] was used for this conversion. The given wavelengths refer to natural neon and may differ by more than the given uncertainties for individual isotopes of neon. Symbol *p* in this column means that the line was predicted but not observed.

[b]Uncertainty of the observed wavelength.

[c]Line character legends: *w* – wide or diffuse or hazy; *c* – complex feature; *s* – shaded to shorter wavelengths; *l* – shaded to longer wavelengths; *bl* – blended with another line that may affect the wavelength and/or intensity (includes "shoulder", "affected" etc.); *m* – masked by other line (no wavelength measured).

[d]An asterisk after the value of uncertainty of the Ritz wavelength means that the upper or lower level of the transition is determined by this line alone. Uncertainties of calculated air wavelengths do not include uncertainties of the fitting formula for the index of refraction of air [21] that was used to obtain them from the calculated wave numbers.

[e]The parent term in parentheses refers to the $2s^22p^4$ configuration of the core.

[f]Difference $\lambda_{obs} - \lambda_{Ritz}$.

[g]References to observed wavelengths: B34 – Boyce 1934 [18]; P71 – Persson 1971 [1]; P83 – Palmer and Engleman 1983 [3]; Q94 – Quinet et al. 1994 [5]; Y85 – Yamada et al. 1985 [20]; HP – this work, Fe/Ne spectrograms taken with roughly 500 Pa of neon (high pressure); MP – this work, Fe/Ne spectrograms taken with roughly (260–400) Pa of neon (medium pressure); N04 – this work, mean of the values obtained from two Cr/Ne and one Pt/Cr/Ne spectrograms.

taken with low currents (15 mA to 20 mA) and long integration times of up to 24 hours. The weighted average of the wave numbers of this line measured on these spectrograms is $37117.390 \pm 0.003\,\mathrm{cm}^{-1}$, which corresponds to the air wavelength 2693.3555 ± 0.0003 Å.

Three extreme ultraviolet (EUV) lines at 331.06 Å, 331.50 Å, and 355.848 Å were listed by Persson [1] with reference to Boyce [18]. This old paper [18] is the only published evidence of their existence.

Wavelengths of 361 infrared lines in the region 1.1 μm to 5.2 μm (1900 cm^{-1} to 9000 cm^{-1}) are taken from Quinet et al. [5]. Although their FTS measurements overlap with those of Palmer and Engleman [5] at shorter wavelengths, data from Quinet et al. [5] in most cases are more precise because of significantly greater signal-to-noise ratios. Since the spectra measured by Quinet et al. [5] were calibrated against the scale of Norlén [12], we applied the wavelength-scale correction to them, which is similar to the correction we did for our Fe/Ne spectra. Namely, we decreased the measured wavelengths by $6.7 \times 10^{-8}\lambda$ in order to bring them to the more accurate scale of Whaling et al. [13]. In terms of wave numbers, this

correction was very small, 0.0001 cm^{-1} to 0.0006 cm^{-1}. Thus, it does not contradict with the statement in reference [5] that the scales of Norlén [12] and Whaling et al. [13] are in very good agreement in the spectral region studied by Quinet et al. [5]. It should be noted that we used the air wavelengths from Quinet et al. [5] to derive the wave numbers of the lines using Edlén's formula for the refraction index of air [19], as it was used by Quinet et al. [5] for the reverse procedure. This was necessary since the wave numbers were given in Quinet et al. [5] with only three digits after the decimal point, while the wavelengths (also given with three digits after the decimal point) have higher relative precision. According to a private communication from the authors of reference [5], the wave numbers were rounded in the process of publication. Therefore, despite the fact that the original quantities measured by Quinet et al. [5] were wave numbers, we used the air wavelengths given therein as primary quantities.

We have discarded four weak lines listed by Quinet et al. [5] at 16872.192 Å, 18626.809 Å, 28029.601 Å, and 38777.281 Å, because they deviate too much from the Ritz wavelengths derived from the optimized level values. The predicted wavelengths for the $(^3P)5p\ ^4D^\circ_{5/2} - (^3P)5d\ ^2F_{5/2}$, $(^3P_2)5f\ [5]^\circ_{11/2} - (^3P_2)6g\ [5]_{11/2}$, $(^3P)5s\ ^2P_{1/2} - (^3P)5p\ ^2S^\circ_{1/2}$, and $(^1D)3d\ ^2P_{3/2} - (^3P_2)4f\ [1]^\circ_{1/2}$ transitions to which these lines were assigned by Quinet et al. [5] are 16872.279 ± 0.003 Å, 18627.151 ± 0.019 Å, 28029.969 ± 0.007 Å, and 38778.22 ± 0.14 Å, respectively. The deviations are much greater than the corresponding line widths.

We changed the identification of the weak line at 38563.66 Å [5] from $(^3P_2)4f\ [1]^\circ_{3/2} - (^1D)3d\ ^2P_{1/2}$ to $(^3P)5d\ ^4P_{5/2} - (^3P)6p\ ^4D^\circ_{5/2}$ because the predicted wavelength for the old classification (38563.12 ± 0.09 Å) was too far from the observed wavelength, while the new classification fits perfectly in the optimized level scheme. The new classification is also in better agreement with the calculated transition probabilities.

Precise measurement of the forbidden transition within the ground term, located at 12.81355 μm, was done by Yamada et al. [20] by means of diode laser spectroscopy.

A few misprints have been found in the line lists of Persson [1] and Quinet et al. [5]. For example, the wavelength 2314.247 Å [1] is the calculated vacuum wavelength instead of the observed air wavelength. The correct wavelength is 2313.551 Å as follows from the given observed wave number 43210.32 cm^{-1}. The classification of the line at 22981.374 Å (4350.162 cm^{-1}) was given as $(^1D)4d\ ^2F_{5/2} - (^3P)5p\ ^4D^\circ_{7/2}$ [5]. This is a misprint; $(^3P)4d\ ^2F_{5/2} - (^3P)5p\ ^4D^\circ_{7/2}$ should be used instead. The correct classification of the line at 19055.735 Å (5246.331 cm^{-1}) [5] is $(^3P)4d\ ^2F_{5/2} - (^3P)5p\ ^4S^\circ_{3/2}$ instead of $(^3P)4d\ ^2F_{3/2} - (^3P)5p\ ^4S^\circ_{3/2}$. A number of line classifications given in Quinet et al. [5] had reversed upper and lower levels. These misprints have been corrected here in Table 1.

The air wavelengths in Table 1 (both observed and Ritz) were derived from the corresponding vacuum wave numbers by means of the five-parameter formula of Peck and Reeder [21] for the refractive index of air. Although the usual practice is to give the wavelengths in the far infrared region above 20000 Å in vacuum and in units of μm, we give all such wavelengths up to 52000 Å in standard air and in units of angstroms, since they were originally given so by Quinet et al. [5]. The uncertainties of the Ritz wavelengths in the air region (2000 Å to 52000 Å) do not include the uncertainties of the refractive index of air.

When using the observed and Ritz wavelengths from Table 1, one should take into account the fact that all the lines were observed for natural neon, which is a mixture of several isotopes. For the spectra produced with pure neon isotopes, the wavelengths may be shifted by amounts considerably exceeding the indicated uncertainties.

The observed relative line intensities given in Table 1 are only approximate. In most cases they are rough visual estimates of the blackening of photographic plates and do not account for variation of the apparatus sensitivity with wavelength. Nevertheless, they are useful for qualitative comparisons and often provide a good criterion for identification of the lines. Since most of the Ne II lines were observed by Persson [1], we used the line intensities given by him to construct a uniform intensity scale for all observed lines. In order to bring the intensities to the same scale as used in the Ne III compilation (Kramida and Nave [11]), the intensities from Persson [1] and Boyce [18] were converted as $I_{\rm new} = 20I_{\rm old} + 2$. The intensities from Quinet et al. [5] were divided by ten. After this conversion, all the experimental spectra appear to be on the same intensity scale throughout the whole spectral region.

5 Wavelength uncertainties

The wavelength measurement uncertainties of the lines listed by Persson [1] were carefully analyzed and discussed in detail therein. Special care was given to the measurement of the two resonance lines at 460.7284 Å and 462.3908 Å. These lines were measured with uncertainty ± 0.0003 Å corresponding to ± 0.14 cm^{-1}.

The uncertainties (one standard deviation) of the wave numbers measured by FTS are characterized by the following formula:

$$\delta\sigma = (\delta\sigma_{\rm stat}^2 + \delta\sigma_{\rm r}^2)^{1/2}, \qquad (1)$$

where $\delta\sigma_{\rm stat}$ is the statistical uncertainty, and $\delta\sigma_{\rm r}$ is the residual uncertainty, which is a combination of the calibration uncertainty and other systematic errors such as illumination shifts (see, for example, Nave et al. [6]). As explained in Kramida and Nave [11], the statistical uncertainties for the neon lines in the FTS spectra that were optimized for measurement of metal lines (belonging to the material of which the cathode is made) are approximately described by the following relation:

$$\delta\sigma_{\rm stat(Ne)} \approx 0.5W(S/N)^{-1}(M_{\rm Ne}/M_{\rm metal})^{1/4}, \qquad (2)$$

where W is the line width (FWHM), S/N is the signal-to-noise ratio, and $M_{\rm Ne}/M_{\rm metal}$ is the ratio of atomic weights of neon and the metal atoms. The factor $(M_{\rm Ne}/M_{\rm metal})^{1/4}$ accounts for the increased number of data points for the wider Doppler line width of neon lines compared to the metal lines. For our Fe/Ne spectra, the value of $\delta\sigma_{\rm stat}$ varied between 0.0001 cm^{-1} for the strongest Ne II lines and 0.17 cm^{-1} for the weakest lines.

The residual uncertainty $\delta\sigma_{\rm r}$, according to Nave et al. [6], was approximately $5 \times 10^{-8}\sigma$ for the visible and near infrared regions and $1 \times 10^{-7}\sigma$ for the VUV and UV regions. Total uncertainty of the measured wave numbers ranged from 0.001 cm^{-1} for the strongest lines to 0.17 cm^{-1} for the weakest lines, with an rms mean of 0.03 cm^{-1}.

As noted above, the FTS data sets used in this work were by-products of studies devoted to other elements, usually heavy metals. The measurement uncertainties of the neon lines were not thoroughly analyzed in Palmer and Engleman [3]. It was only noted there that they were, on average, three times greater than the uncertainties of the thorium lines. Nevertheless, the data presented by Palmer and Engleman [3] are sufficient to estimate these uncertainties. We estimated the noise level for each of the Ne II lines from the complete set of spectrograms contained in the thorium-neon atlas [3]. The wave numbers and intensities of all neon lines are given in Appendix B of Palmer and Engleman [3]. The line width of the neon lines (full width at half maximum) was 0.11 cm^{-1} at wave numbers around 16500 cm^{-1}. This corresponds to the relative width $\Delta\lambda/\lambda = 6.7 \times 10^{-6}$. Based on the discussion in Palmer and Engleman [3], we assumed that the relative widths of the lines remained constant with varying wavelength, as they were defined by Doppler broadening. We estimated the number of statistically independent data points per FWHM by dividing the Doppler line width by the theoretical spectral resolution given in Table IV of Palmer and Engleman [3]. Throughout the entire spectral range, this number varied between 3 and 5 with an average of 4. Therefore, the statistical uncertainty of the Ne II lines measured by Palmer and Engleman [3] is sufficiently well described by the simplified equation

$$\delta\sigma_{\rm stat(Ne/Th)} \approx W/(2\,S/N) \qquad (3)$$

with the line width W defined by Doppler broadening, $W = 6.7 \times 10^{-6}\sigma$ (see Eq. (1) in Kramida and Nave [11]). The residual uncertainty $\delta\sigma_{\rm r}$, according to Palmer and Engleman [3], was approximately $5 \times 10^{-8}\sigma$ for the entire spectral region.

From these considerations, we found that the measurement uncertainties of the Ne II lines observed by Palmer and Engleman [3] vary from 0.0007 cm^{-1} for the strong isolated lines to 0.03 cm^{-1} for the weakest lines, with an average of 0.008 cm^{-1}. In terms of wavelength, it corresponds to uncertainties of 0.0002 Å to 0.008 Å with an average of 0.0016 Å.

Information about the line widths and signal-to-noise ratios of the infrared lines listed in Quinet et al. [5] was furnished by Quinet [22]. In this work, FT spectra of V/Ne/Ar and Mg/Ne/Ar hollow cathodes were used in the regions 1800 cm^{-1} to 3800 cm^{-1} and 3800 cm^{-1} to 9000 cm^{-1}, respectively. The relative line widths in these spectra were $\Delta\lambda/\lambda = 8 \times 10^{-6}$ and 5×10^{-6}, respectively. Although these relative line widths were about the same as in our Fe/Ne spectra, the absolute widths of the Ne II lines in terms of wave numbers were much smaller in Quinet et al. [5] because of the longer wavelength range. A typical line width at 20000 Å (5000 cm^{-1}) was only 0.025 cm^{-1} in the Mg/Ne/Ar spectrum [5], compared with the typical width of 0.27 cm^{-1} at 3000 Å in our Fe/Ne spectrum.

We determined the statistical uncertainty of the wave numbers measured by Quinet et al. [5] in a similar way as we did for the Th/Ne spectrum [3]. Namely, we determined the number of statistically independent data points per line width ($N_{\rm w}$) as FWHM divided by the spectral resolution of the spectrometer used by Quinet et al. [5]. We obtained the details of the observing parameters for these spectra from the Kitt Peak archives at `http://diglib.nso.edu`. The dates of the spectra used in reference [5] are given in Biémont and Brault [4]. From these data, it follows that the spectral resolution of the spectrometer was 0.011 cm^{-1}. The obtained values of $N_{\rm w}$ vary between 2 and 5. Then the statistical uncertainty was determined as follows:

$$\delta\sigma_{\rm stat(Ne/Mg,Ne/V)} \approx W/[(S/N)N_{\rm w}^{1/2}] \qquad (4)$$

(see Eq. (3) in Kramida and Nave [11]). We combined the uncertainties resulting from equation (4) (by means of the square root of the sum of squares) with an additional uncertainty resulting from rounding of the wavelengths listed in Quinet et al. [5]. The rounding error should be taken into account because the original precisely measured wave numbers, as explained in the previous section, are not available. It is the largest for the shortest wavelength (11226.948 Å) where it amounts to 2×10^{-4} cm^{-1} and smallest for the longest wavelength (51321.50 Å), where it is only 1×10^{-5} cm^{-1}.

The residual uncertainty $\delta\sigma_{\rm r}$ for the spectra used by Quinet et al. [5] was analyzed in Biémont and Brault [4] (where these spectra were originally obtained) by comparing the measured Ar I lines with interferometric measurements of Norlén [12] used for calibration. As stated by Biémont and Brault [4], the measured and reference wave numbers differed by a few 10^{-4} cm^{-1}. We assumed $\delta\sigma_{\rm r} = 5 \times 10^{-4}$ cm^{-1} for the entire spectral region 1900 cm^{-1} to 9000 cm^{-1} covered in Quinet et al. [5].

For the lines noted in Quinet et al. [5] as blended, we assumed the measurement uncertainty equal to half of FWHM. For the wide lines belonging to unresolved $5g-6h$ transitions, even though they were not marked as blended, we assumed the measurement uncertainty to be equal to the difference between the measured line width and the Doppler width.

The total estimated uncertainty for the lines measured by Quinet et al. [5] varies between 0.0005 cm^{-1} for the strongest lines and 0.02 cm^{-1} for the weakest or blended lines, with an average of 0.006 cm^{-1}.

6 Energy levels and calculated wavelengths

To obtain the energy levels that would best fit to all observed lines, we have used the level optimization code LOPT described in Kramida and Nave [11]. This code calculates the best values of the energy levels by performing a weighted least-squares fit of the differences between the upper and the lower levels of the transitions to the observed wave numbers.. The weights are equal to the squares of the reciprocal wave-number uncertainties. The list of optimized energy level values is given in Table 2. The level uncertainties given in Table 2 were also calculated by the LOPT code. The positions of all excited states with principal quantum number 3 or greater are very accurately determined relative to the levels of the $(^3\mathrm{P})3s\,^4\mathrm{P}$ term, of which the $^4\mathrm{P}_{3/2}$ level has the largest number of accurately measured transitions (19). Hence, uncertainties of all levels with $n \geq 3$ are given relative to the $(^3\mathrm{P})3s\,^4\mathrm{P}_{3/2}$ level. The position of the $n = 3$ configurations relative to the first excited configuration, $2s2p^6$, is determined by the $2s2p^6\,^2\mathrm{S}_{1/2}$ – $(^3\mathrm{P})3p\,^2\mathrm{P}^\circ_{3/2}$ line at 2693.3555 ± 0.0003 Å (see Sect. 4). This uncertainty corresponds to a wave-number uncertainty of ± 0.004 cm^{-1}. The uncertainty of the $(^3\mathrm{P})3s\,^4\mathrm{P}_{3/2}$ level, which is given in Table 2 relative to the $2s2p^6\,^2\mathrm{S}_{1/2}$ level, is mainly determined by the above-mentioned line and is only slightly increased by uncertainties of connections within the $n = 3$ configurations. The uncertainty of the $2s^22p^5\,^2\mathrm{P}^\circ_{1/2}$ level relative to the ground state (0.002 cm^{-1}) is due to the precise measurement of the forbidden $J = 3/2 - 1/2$ transition within the ground term by Yamada et al. [20]. The position of the $2s2p^6\,^2\mathrm{S}_{1/2}$ level relative to the ground state is determined by the two resonance lines at 460.7284 Å and 462.3908 Å that were precisely measured by Persson [1]. According to Persson, the measurement uncertainty of these two lines is 0.14 cm^{-1}. In addition to these two lines, the $n = 3$ levels are connected to the ground term by the lines at 405.8538 Å, 407.1376 Å, 445.0397 Å, 446.2556 Å, 446.5901 Å, and 447.8150 Å, measured by Persson [1] with uncertainties between 0.5 cm^{-1} and 0.6 cm^{-1}. Taking into account the above-mentioned line at 2693.3555 ± 0.0003 Å, which precisely determines the position of the $n = 3$ levels relative to the $2s2p^6\,^2\mathrm{S}_{1/2}$ level, the combined statistical effect of these lines reduces the uncertainty of the $2s2p^6\,^2\mathrm{S}_{1/2}$ level relative to the ground level to ± 0.09 cm^{-1}. To determine the uncertainties of the levels with $n \geq 3$ relative to the ground state, one must combine in quadrature the level uncertainty value given in Table 2 with the uncertainty of the $2s2p^6\,^2\mathrm{S}_{1/2}$ level.

Despite the fact that the uncertainties of most of the higher levels relative to the $(^3\mathrm{P})3s\,^4\mathrm{P}_{3/2}$ level are 0.002 cm^{-1} or greater, many of the levels are given in Table 2 with four digits after the decimal point. The extra digit is necessary to reproduce the precisely measured wave numbers of the lines that involve these levels. Thus, the number of given decimal places in the level value is determined by the *minimum relative uncertainty* of this level, which is the smallest uncertainty of the Ritz wave number of any observed transition involving this level. The level values were rounded so that the minimum relative uncertainty of each level is between 2 and 15 units of the last given decimal place. For example, the levels having minimum relative uncertainties greater than 0.015 cm^{-1} but smaller than 0.15 cm^{-1} are given with two digits after the decimal point. Similarly, the levels having minimum relative uncertainties between 0.0015 cm^{-1} and 0.015 cm^{-1} are given with three digits after the decimal point.

The level designations given in Table 2 in most cases are the same as given by Persson [1]. Designations of 18 levels were changed based on the results of our parametric fitting (described in the following section). The percentage compositions given in Table 2 also result from our calculations.

Our optimized level values given in Table 2 agree very well with the energies given by Persson [1] and Quinet et al. [5]. The largest difference between our and Persson's level values [1] is -0.12 cm^{-1} with a mean difference -0.021 cm^{-1} and a standard deviation from this mean 0.019 cm^{-1}. Similarly, the largest difference between our level values and those given by Quinet et al. [5] is -0.06 cm^{-1} with a mean difference of -0.021 cm^{-1} and a standard deviation from this mean of 0.014 cm^{-1}. These differences are smaller than the level uncertainties stated in Persson [1] and Quinet et al. [5] and do not affect the values of the ionization limits found by Persson [1].

In addition to finding the optimized level values, the LOPT code calculates the uncertainties of the calculated (Ritz) wavelengths for all observed lines. These uncertainties are given in Table 1 along with the uncertainties of the observed wavelengths.

For the infrared lines measured by Quinet et al. [5], the Ritz wavelengths calculated using the level values from Persson [1] and Quinet et al. [5] deviate from the observed wavelengths, on average, by 0.7 of the line width, while the average uncertainty of the observed wavelengths was only 0.16 of the line width. About fifty lines deviated by more than the line width from the Ritz wavelengths. Reduction of these large deviations was one of the main motivations of the present work. With our new level values the standard deviation of the Ritz wavelengths of these infrared lines from the ones observed in reference [5] decreased to 0.09 of the line width, which is entirely consistent with the wavelength-measurement uncertainties.

To estimate the quality of the optimized levels, we compared the line deviations (Ritz wave numbers minus observed ones) with the measurement uncertainties by calculating the rms values of their ratios for each set of measurements. Table 3 gives a summary of this comparison. When calculating these rms values, we excluded the lines that alone determine the upper or lower level of the transition.

As seen from the last column of Table 3, the mean ratios of the wave number deviations to the measurement uncertainties adopted in the present work are reasonably close to 1.0 for the lines measured in Palmer and Engleman [3] and in this work, and are 0.5 to 0.6 for the lines from Persson [1], Quinet et al. [5], and Boyce [18].

Table 2. Energy levels of Ne II.

Configuration	Term	J	Level (cm^{-1})	Uncert.[a] (cm^{-1})	Leading percentages[b]		
$2s^2 2p^5$	^{2}P°	3/2	0.0000	–	100%		
		1/2	780.4240	0.002	100%		
$2s2p^6$	^{2}S	1/2	217047.598	0.09	98%		
$2s^2 2p^4(^3\mathrm{P})3s$	^{4}P	5/2	219130.7609	0.0011	100%		
		3/2	219648.4248	0.005	100%		
		1/2	219947.4453	0.0011	100%		
$2s^2 2p^4(^3\mathrm{P})3s$	^{2}P	3/2	224087.0092	0.0013	100%		
		1/2	224699.2716	0.0014	100%		
$2s^2 2p^4(^3\mathrm{P})3p$	^{4}P°	5/2	246192.4130	0.0014	99%		
		3/2	246415.0144	0.0011	99%		
		1/2	246597.6805	0.0012	100%		
$2s^2 2p^4(^1\mathrm{D})3s$	^{2}D	5/2	246394.1202	0.0015	100%		
		3/2	246397.4810	0.002	100%		
$2s^2 2p^4(^3\mathrm{P})3p$	^{4}D°	7/2	249108.6138	0.0014	100%		
		5/2	249445.9632	0.0012	98%		
		3/2	249695.5051	0.0013	99%		
		1/2	249839.6186	0.0014	100%		
$2s^2 2p^4(^3\mathrm{P})3p$	^{2}D°	5/2	251011.1511	0.0015	99%		
		3/2	251522.0967	0.0015	99%		
$2s^2 2p^4(^3\mathrm{P})3p$	^{2}S°	1/2	252798.4654	0.002	93%	+ 6%	$(^3\mathrm{P})3p\,^2\mathrm{P}°$
$2s^2 2p^4(^3\mathrm{P})3p$	^{4}S°	3/2	252953.5198	0.0013	99%		
$2s^2 2p^4(^3\mathrm{P})3p$	^{2}P°	3/2	254164.9888	0.0014	92%	+ 6%	$(^1\mathrm{D})3p\,^2\mathrm{P}°$
		1/2	254292.1683	0.0015	86%	+ 7%	$(^1\mathrm{D})3p\,^2\mathrm{P}°$
$2s^2 2p^4(^1\mathrm{D})3p$	^{2}F°	5/2	274364.5596	0.002	100%		
		7/2	274409.0830	0.002	100%		
$2s^2 2p^4(^1\mathrm{D})3p$	^{2}P°	3/2	276276.8361	0.002	89%	+ 5%	$(^3\mathrm{P})3p\,^2\mathrm{P}°$
		1/2	276511.800	0.003	89%	+ 6%	$(^3\mathrm{P})3p\,^2\mathrm{P}°$
$2s^2 2p^4(^1\mathrm{S})3s$	^{2}S	1/2	276677.1142	0.003	97%		
$2s^2 2p^4(^1\mathrm{D})3p$	^{2}D°	3/2	277325.5757	0.003	100%		
		5/2	277344.2675	0.002	100%		
$2s^2 2p^4(^3\mathrm{P})3d$	^{4}D	7/2	279137.6053	0.003	96%		
		5/2	279218.6416	0.002	94%		
		3/2	279324.8733	0.002	95%		
		1/2	279422.869	0.003	97%		
$2s^2 2p^4(^3\mathrm{P})3d$	^{4}F	9/2	280172.9854	0.003	100%		
		7/2	280700.7426	0.002	52%	+ 44%	$(^3\mathrm{P})3d\,^2\mathrm{F}$
		5/2	280797.2387	0.002	72%	+ 24%	$(^3\mathrm{P})3d\,^2\mathrm{D}$
		3/2	280947.0768	0.002	63%	+ 27%	$(^3\mathrm{P})3d\,^4\mathrm{P}$
$2s^2 2p^4(^3\mathrm{P})3d$	^{2}F	7/2	280262.3163	0.003	55%	+ 45%	$(^3\mathrm{P})3d\,^4\mathrm{F}$
		5/2	281025.9326	0.002	67%	+ 19%	$(^3\mathrm{P})3d\,^4\mathrm{P}$

Table 2. *Continued.*

Configuration	Term	J	Level (cm^{-1})	Uncert.[a] (cm^{-1})	Leading percentages[b]		
$2s^2 2p^4(^3P)3d$	^2D	5/2	280268.9453	0.003	58%	+ 21%	$(^3P)3d\,^2F$
		3/2	280473.5550	0.002	68%	+ 18%	$(^3P)3d\,^4F$
$2s^2 2p^4(^3P)3d$	^4P	1/2	280768.508	0.002	96%		
		3/2	280989.5229	0.002	58%	+ 21%	$(^3P)3d\,^2D$
		5/2	281171.3566	0.002	64%	+ 12%	$(^3P)3d\,^2D$
$2s^2 2p^4(^3P)3d$	^2P	1/2	281332.521	0.003	96%		
		3/2	281720.2755	0.002	88%	+ 7%	$(^3P)3d\,^2D$
$2s^2 2p^4(^3P)4s$	^4P	5/2	281998.2635	0.002	90%	+ 10%	$(^3P)3d\,^4P$
		3/2	282375.3049	0.002	91%	+ 5%	$(^3P)4s\,^2P$
		1/2	282680.6284	0.002	97%		
$2s^2 2p^4(^3P)4s$	^2P	3/2	283322.3319	0.002	93%	+ 5%	$(^3P)4s\,^4P$
		1/2	283894.3965	0.002	98%		
$2s^2 2p^4(^3P)4p$	$^4P^\circ$	5/2	290371.9268	0.002	95%	+ 5%	$(^3P)4p\,^4D^\circ$
		3/2	290583.1503	0.002	94%		
		1/2	290803.7989	0.002	97%		
$2s^2 2p^4(^3P)4p$	$^4D^\circ$	7/2	291202.0096	0.003	100%		
		5/2	291495.0176	0.002	80%	+ 17%	$(^3P)4p\,^2D^\circ$
		3/2	291801.858	0.003	91%	+ 5%	$(^3P)4p\,^2D^\circ$
		1/2	291968.116	0.003	98%		
$2s^2 2p^4(^3P)4p$	$^2D^\circ$	5/2	292033.1263	0.003	83%	+ 15%	$(^3P)4p\,^4D^\circ$
		3/2	292451.7592	0.002	93%	+ 6%	$(^3P)4p\,^4D^\circ$
$2s^2 2p^4(^3P)4p$	$^2S^\circ$	1/2	292546.687	0.003	95%		
$2s^2 2p^4(^3P)4p$	$^4S^\circ$	3/2	292651.298	0.006	96%		
$2s^2 2p^4(^3P)4p$	$^2P^\circ$	3/2	294086.4608	0.002	91%		
		1/2	294333.192	0.003	90%		
$2s^2 2p^4(^3P)4d$	^4D	7/2	301801.0594	0.003	87%	+ 11%	$(^3P)4d\,^4F$
		5/2	301855.6707	0.003	84%	+ 8%	$(^3P)4d\,^4P$
		3/2	301947.9789	0.003	81%	+ 13%	$(^3P)4d\,^4P$
		1/2	302057.2516	0.003	83%	+ 11%	$(^3P)4d\,^4P$
$2s^2 2p^4(^3P)4d$	^4F	9/2	302192.9098	0.003	100%		
		7/2	302750.7840	0.003	58%	+ 30%	$(^3P)4d\,^2F$
		5/2	302839.2693	0.003	60%	+ 24%	$(^3P)4d\,^2D$
		3/2	302961.0417	0.003	78%	+ 15%	$(^3P)4d\,^2P$
$2s^2 2p^4(^3P)4d$	^2F	7/2	302247.7634	0.003	68%	+ 31%	$(^3P)4d\,^4F$
		5/2	302890.5369	0.003	38%	+ 25%	$(^3P)5s\,^4P$
$2s^2 2p^4(^3P)4d$	^2D	5/2	302307.7230	0.003	54%	+ 23%	$(^3P)4d\,^2F$
		3/2	302425.8139	0.003	44%	+ 31%	$(^3P)4d\,^4P$
$2s^2 2p^4(^3P)4d$	^4P	1/2	302475.5806	0.003	81%	+ 13%	$(^3P)4d\,^2P$
		3/2	302816.9602	0.003	52%	+ 24%	$(^3P)4d\,^2D$
		5/2	303071.8002	0.003	47%	+ 30%	$(^3P)4d\,^2F$
$2s^2 2p^4(^3P_2)4f$	$[4]^\circ$	9/2	302829.0453	0.004	99%		

Table 2. *Continued.*

Configuration	Term	J	Level (cm^{-1})	Uncert.[a] (cm^{-1})	Leading percentages[b]		
		7/2	302831.176	0.003	96%		
$2s^2 2p^4(^3P)4d$	^2P	1/2	302831.7640	0.003	78%	+ 12%	$(^3P)4d\,^4D$
		3/2	303237.8943	0.003	57%	+ 24%	$(^3P)4d\,^2D$
$2s^2 2p^4(^3P_2)4f$	$[3]^\circ$	7/2	302843.509	0.004	96%		
		5/2	302844.085	0.003	99%		
$2s^2 2p^4(^3P_2)4f$	$[2]^\circ$	3/2	302902.557	0.004	98%		
		5/2	302903.635	0.004	98%		
$2s^2 2p^4(^3P_2)4f$	$[5]^\circ$	9/2	302935.2919	0.003	100%		
		11/2	302935.312	0.004	100%		
$2s^2 2p^4(^3P_2)4f$	$[1]^\circ$	1/2	302988.859	0.009	100%		
		3/2	302989.805	0.004	100%		
$2s^2 2p^4(^3P)5s$	^4P	5/2	303279.8915	0.003	65%	+ 24%	$(^3P)4d\,^4P$
		3/2	303518.1843	0.003	61%	+ 29%	$(^3P)5s\,^2P$
		1/2	303928.0756	0.003	92%	+ 7%	$(^3P)5s\,^2P$
$2s^2 2p^4(^3P_1)4f$	$[2]^\circ$	3/2	303508.458	0.004	98%		
		5/2	303509.514	0.003	98%		
$2s^2 2p^4(^3P_1)4f$	$[4]^\circ$	9/2	303527.7267	0.003	99%		
		7/2	303528.5122	0.003	99%		
$2s^2 2p^4(^3P_1)4f$	$[3]^\circ$	7/2	303599.9098	0.003	100%		
		5/2	303600.498	0.004	100%		
$2s^2 2p^4(^3P_0)4f$	$[3]^\circ$	7/2	303824.2119	0.003	99%		
		5/2	303824.6705	0.003	99%		
$2s^2 2p^4(^3P)5s$	^2P	3/2	303974.2630	0.003	64%	+ 34%	$(^3P)5s\,^4P$
		1/2	304440.2089	0.003	92%	+ 7%	$(^3P)5s\,^4P$
$2s^2 2p^4(^1D)3d$	^2G	9/2	305364.004	0.003	100%		
		7/2	305365.116	0.004	100%		
$2s^2 2p^4(^1S)3p$	$^2P^\circ$	3/2	305398.5968	0.003	92%	+ 5%	$(^3P)5p\,^2P^\circ$
		1/2	305408.498	0.005	93%		
$2s^2 2p^4(^1D)3d$	^2P	3/2	305566.923	0.003	97%		
		1/2	305582.249	0.005	97%		
$2s^2 2p^4(^1D)3d$	^2S	1/2	306011.056	0.003	98%		
$2s^2 2p^4(^1D)3d$	^2D	5/2	306243.4077	0.003	96%		
		3/2	306262.755	0.004	96%		
$2s^2 2p^4(^1D)3d$	^2F	5/2	306687.271	0.003	100%		
		7/2	306687.654	0.003	100%		
$2s^2 2p^4(^3P)5p$	$^4P^\circ$	5/2	306899.2903	0.003	88%	+ 11%	$(^3P)5p\,^4D^\circ$
		3/2	307069.8080	0.003	83%	+ 9%	$(^3P)5p\,^4S^\circ$
		1/2	307309.4584	0.003	85%	+ 10%	$(^3P)5p\,^2S^\circ$
$2s^2 2p^4(^3P)5p$	$^4D^\circ$	7/2	307240.7001	0.003	100%		
		3/2	307774.6858	0.003	63%	+ 21%	$(^3P)5p\,^2D^\circ$

Table 2. *Continued.*

Configuration	Term	J	Level (cm^{-1})	Uncert.[a] (cm^{-1})	Leading percentages[b]		
		5/2	307894.8198	0.003	45%	+ 46%	$(^3P)5p\,^2D^\circ$
		1/2	308022.9587	0.003	94%		
$2s^22p^4(^3P)5p$	$^2D^\circ$	5/2	307420.8248	0.003	53%	+ 44%	$(^3P)5p\,^4D^\circ$
		3/2	308177.1843	0.003	65%	+ 26%	$(^3P)5p\,^4D^\circ$
$2s^22p^4(^3P)5p$	$^2S^\circ$	1/2	308006.8460	0.003	82%	+ 11%	$(^3P)5p\,^4P^\circ$
$2s^22p^4(^1D)4s$	^2D	5/2	308101.2468	0.003	97%		
		3/2	308101.6076	0.003	97%		
$2s^22p^4(^3P)5p$	$^4S^\circ$	3/2	308136.8685	0.003	78%	+ 12%	$(^3P)5p\,^4P^\circ$
$2s^22p^4(^3P)5p$	$^2P^\circ$	3/2	308738.0108	0.003	75%	+ 11%	$(^3P)5p\,^2D^\circ$
		1/2	308976.8347	0.003	82%	+ 8%	$(^3P)5p\,^2S^\circ$
$2s^22p^4(^3P)5d$	^4D	7/2	312223.5155	0.003	79%	+ 17%	$(^3P)5d\,^4F$
		5/2	312258.0516	0.003	75%	+ 14%	$(^3P)5d\,^4P$
		3/2	312325.6366	0.003	65%	+ 26%	$(^3P)5d\,^4P$
		1/2	312414.9292	0.004	52%	+ 39%	$(^3P)5d\,^4P$
$2s^22p^4(^3P)5d$	^4F	9/2	312407.6220	0.003	100%		
		7/2	312994.3611	0.003	57%	+ 23%	$(^3P)5d\,^2F$
		5/2	313072.2891	0.003	52%	+ 27%	$(^3P)5d\,^2D$
		3/2	313128.5294	0.003	63%	+ 21%	$(^3P)5d\,^2P$
$2s^22p^4(^3P)5d$	^2F	7/2	312440.6573	0.003	73%	+ 26%	$(^3P)5d\,^4F$
		5/2	313346.0878	0.003	33%	+ 27%	$(^3P)5d\,^4P$
$2s^22p^4(^3P)5d$	^2D	5/2	312504.5327	0.003	55%	+ 23%	$(^3P)5d\,^2F$
		3/2	312573.7745	0.003	39%	+ 30%	$(^3P)5d\,^4P$
$2s^22p^4(^3P)5d$	^4P	1/2	312585.170	0.004	51%	+ 35%	$(^3P)5d\,^2P$
		3/2	313021.8155	0.003	40%	+ 27%	$(^3P)5d\,^4D$
		5/2	313138.5238	0.003	41%	+ 30%	$(^3P)5d\,^2F$
$2s^22p^4(^3P_2)5f$	$[4]^\circ$	9/2	312763.8929	0.005	100%		
		7/2	312765.4821	0.004	94%	+ 6%	$(^3P_2)5f[3]^\circ$
$2s^22p^4(^3P_2)5f$	$[3]^\circ$	7/2	312771.9922	0.005	94%	+ 6%	$(^3P_2)5f[4]^\circ$
		5/2	312772.4309	0.005	99%		
$2s^22p^4(^3P_2)5f$	$[2]^\circ$	3/2	312804.0268	0.005	99%		
		5/2	312804.7127	0.005	99%		
$2s^22p^4(^3P_2)5g$	[5]	9/2	312810.675	0.02	100%		
		11/2	312810.682	0.004	100%		
$2s^22p^4(^3P_2)5g$	[4]	7/2	312811.580	0.005	100%		
		9/2	312811.604	0.004	100%		
$2s^22p^4(^3P_2)5f$	$[5]^\circ$	11/2	312816.6500	0.004	100%		
		9/2	312816.689	0.004	100%		
$2s^22p^4(^3P_2)5g$	[3]	5/2	312824.761	0.006	100%		
		7/2	312824.776	0.005	100%		
$2s^22p^4(^3P_2)5g$	[6]	11/2	312833.415	0.006	100%		

Table 2. *Continued.*

Configuration	Term	J	Level (cm^{-1})	Uncert.[a] (cm^{-1})	Leading percentages[b]		
		13/2	312833.433	0.006	100%		
$2s^2 2p^4(^3P_2)5g$	[2]	3/2	312843.10	0.03	100%		
		5/2	312843.122	0.008	100%		
$2s^2 2p^4(^3P_2)5f$	[1]°	1/2	312843.6043	0.008	100%		
		3/2	312844.5547	0.007	100%		
$2s^2 2p^4(^3P)6s$	^4P	5/2	312903.4650	0.003	87%	+ 7%	$(^3P)5d\,^4P$
		3/2	313652.1424	0.003	62%	+ 36%	$(^3P)6s\,^2P$
		1/2	313700.1049	0.003	78%	+ 22%	$(^3P)6s\,^2P$
$2s^2 2p^4(^3P)5d$	^2P	1/2	313006.2024	0.004	55%	+ 34%	$(^3P)5d\,^4D$
		3/2	313425.5082	0.003	48%	+ 28%	$(^3P)5d\,^2D$
$2s^2 2p^4(^3P)6s$	^2P	3/2	313180.2149	0.003	52%	+ 29%	$(^3P)6s\,^4P$
		1/2	314018.9129	0.003	78%	+ 22%	$(^3P)6s\,^4P$
$2s^2 2p^4(^3P_1)5f$	[2]°	3/2	313419.0375	0.02	99%		
		5/2	313420.0366	0.006	99%		
$2s^2 2p^4(^3P_1)5f$	[4]°	9/2	313431.469	0.005	100%		
		7/2	313432.262	0.006	100%		
$2s^2 2p^4(^3P_1)5g$	[3]	5/2	313457.5072	0.006	100%		
		7/2	313457.5580	0.02	100%		
$2s^2 2p^4(^3P_1)5g$	[5]	9/2	313461.954	0.02	100%		
		11/2	313461.962	0.004	100%		
$2s^2 2p^4(^3P_1)5f$	[3]°	7/2	313469.9028	0.006	100%		
		5/2	313470.4054	0.008	100%		
$2s^2 2p^4(^3P_1)5g$	[4]	7/2	313480.181	0.005	100%		
		9/2	313480.213	0.004	100%		
$2s^2 2p^4(^3P_0)5f$	[3]°	7/2	313718.9516	0.007	100%		
		5/2	313719.3496	0.013	100%		
$2s^2 2p^4(^3P_0)5g$	[4]	7/2	313744.493	0.004	100%		
		9/2	313744.54	0.03	100%		
$2s^2 2p^4(^3P)6p$	$^4P°$	5/2	314927.6979	0.004	83%	+ 16%	$(^3P)6p\,^4D°$
		3/2	315040.109	0.004	70%	+ 17%	$(^3P)6p\,^4S°$
		1/2	315600.112	0.005	50%	+ 26%	$(^3P)6p\,^2P°$
$2s^2 2p^4(^3P)6p$	$^2S°$	1/2	315241.372	0.004	32%	+ 45%	$(^3P)6p\,^4P°$
$2s^2 2p^4(^3P)6p$	$^4D°$	7/2	315099.9990	0.003	100%		
		5/2	315730.9311	0.004	56%	+ 30%	$(^3P)6p\,^2D°$
		1/2	315821.061	0.004	68%	+ 23%	$(^3P)6p\,^2S°$
$2s^2 2p^4(^3P)6p$	$^2D°$	5/2	315202.7541	0.004	69%	+ 28%	$(^3P)6p\,^4D°$
		3/2	316052.5791	0.004	47%	+ 14%	$(^3P)6p\,^4D°$
$2s^2 2p^4(^3P)6p$	$^4S°$	3/2	315854.611	0.004	53%	+ 30%	$(^3P)6p\,^2D°$
$2s^2 2p^4(^1D)4p$	$^2F°$	5/2	316882.1781	0.003	100%		
		7/2	316897.1647	0.003	100%		

Table 2. *Continued.*

Configuration	Term	J	Level (cm^{-1})	Uncert.[a] (cm^{-1})	Leading percentages[b]		
$2s^2 2p^4(^1\mathrm{D})4p$	$^2\mathrm{P}^\circ$	3/2	317663.1046	0.003	63%	+ 13%	$(^3\mathrm{P})7p\,^2\mathrm{P}^\circ$
		1/2	317828.3130	0.003	65%	+ 17%	$(^3\mathrm{P})6p\,^2\mathrm{P}^\circ$
$2s^2 2p^4(^1\mathrm{D})4p$	$^2\mathrm{D}^\circ$	5/2	317781.404	0.005	100%		
		3/2	317781.767	0.006	94%		
$2s^2 2p^4(^3\mathrm{P})6d$	$^4\mathrm{D}$	7/2	317840.185	0.004	74%	+ 22%	$(^3\mathrm{P})6d\,^4\mathrm{F}$
		5/2	317862.246	0.005	69%	+ 18%	$(^3\mathrm{P})6d\,^4\mathrm{P}$
		3/2	317907.053	0.005	55%	+ 35%	$(^3\mathrm{P})6d\,^4\mathrm{P}$
$2s^2 2p^4(^3\mathrm{P})6d$	$^4\mathrm{F}$	9/2	317940.958	0.004	100%		
		7/2	318413.305	0.004	54%	+ 25%	$(^3\mathrm{P})6d\,^4\mathrm{D}$
$2s^2 2p^4(^3\mathrm{P})6d$	$^2\mathrm{F}$	7/2	317961.309	0.004	76%	+ 24%	$(^3\mathrm{P})6d\,^4\mathrm{F}$
$2s^2 2p^4(^3\mathrm{P})6d$	$^2\mathrm{D}$	5/2	318000.208	0.007	59%	+ 21%	$(^3\mathrm{P})6d\,^2\mathrm{F}$
$2s^2 2p^4(^3\mathrm{P}_2)6f$	$[4]^\circ$	9/2	318156.0520	0.003	100%		
		7/2	318157.1429	0.003	92%	+ 8%	$(^3\mathrm{P}_2)6f[3]^\circ$
$2s^2 2p^4(^3\mathrm{P}_2)6f$	$[3]^\circ$	7/2	318160.9720	0.003	92%	+ 8%	$(^3\mathrm{P}_2)6f[4]^\circ$
		5/2	318161.2874	0.004	99%		
$2s^2 2p^4(^3\mathrm{P}_2)6f$	$[2]^\circ$	3/2	318179.865	0.004	100%		
		5/2	318180.3002	0.004	99%		
$2s^2 2p^4(^3\mathrm{P}_2)6g$	[5]	9/2	318183.6797	0.004	100%		
		11/2	318183.6919	0.005	100%		
$2s^2 2p^4(^3\mathrm{P}_2)6g$	[4]	7/2	318184.2181	0.005	100%		
		9/2	318184.2286	0.005	100%		
$2s^2 2p^4(^3\mathrm{P}_2)6f$	$[5]^\circ$	11/2	318186.1197	0.003	100%		
		9/2	318186.1608	0.003	100%		
$2s^2 2p^4(^3\mathrm{P}_2)6h$	$[5]^\circ$		318190.507	0.012	100%		
$2s^2 2p^4(^3\mathrm{P}_2)6h$	$[6]^\circ$		318190.691	0.014	100%		
$2s^2 2p^4(^3\mathrm{P}_2)6g$	[3]	5/2	318191.9290	0.005	100%		
		7/2	318191.9428	0.005	100%		
$2s^2 2p^4(^3\mathrm{P}_2)6h$	$[4]^\circ$		318194.306	0.011	100%		
$2s^2 2p^4(^3\mathrm{P}_2)6g$	[6]	11/2	318196.72	0.04	100%		
		13/2	318196.7724	0.004	100%		
$2s^2 2p^4(^3\mathrm{P}_2)6h$	$[7]^\circ$		318197.60	0.02	100%		
$2s^2 2p^4(^3\mathrm{P}_2)6h$	$[3]^\circ$		318200.066	0.015	100%		
$2s^2 2p^4(^3\mathrm{P}_2)6f$	$[1]^\circ$	1/2	318201.7	0.2	100%		
		3/2	318202.217	0.006	100%		
$2s^2 2p^4(^3\mathrm{P}_2)6g$	[2]	3/2	318202.3663	0.008	100%		
		5/2	318202.3922	0.007	100%		
$2s^2 2p^4(^3\mathrm{P})7s$	$^4\mathrm{P}$	5/2	318256.108	0.005	98%		

Table 2. *Continued.*

Configuration	Term	J	Level (cm^{-1})	Uncert.[a] (cm^{-1})	Leading percentages[b]		
		3/2	318940.046	0.006	73%	+ 26%	(^{3}P)7s ^{2}P
$2s^2 2p^4(^3\mathrm{P})7s$	^{2}P	3/2	318452.80	0.07	71%	+ 25%	(^{3}P)7s ^{4}P
$2s^2 2p^4(^3\mathrm{P}_1)6f$	[2]°	3/2	318804.327	0.005	100%		
		5/2	318805.121	0.004	100%		
$2s^2 2p^4(^3\mathrm{P}_1)6f$	[4]°	9/2	318812.1133	0.004	100%		
		7/2	318812.7356	0.003	100%		
$2s^2 2p^4(^3\mathrm{P}_1)6g$	[3]	7/2	318828.4917	0.006	100%		
		5/2	318828.4968	0.02	100%		
$2s^2 2p^4(^3\mathrm{P}_1)6g$	[5]	9/2	318831.1565	0.006	100%		
		11/2	318831.1861	0.005	100%		
$2s^2 2p^4(^3\mathrm{P}_1)6h$	[4]°	7/2	318834.4654	0.006	100%		
		9/2	318834.4865	0.02	100%		
$2s^2 2p^4(^3\mathrm{P}_1)6f$	[3]°	7/2	318834.7543	0.004	100%		
		5/2	318835.128	0.004	100%		
$2s^2 2p^4(^3\mathrm{P}_1)6h$	[6]°		318835.64	0.02	100%		
$2s^2 2p^4(^3\mathrm{P}_1)6h$	[5]°		318841.497	0.012	100%		
$2s^2 2p^4(^3\mathrm{P}_1)6g$	[4]	7/2	318841.8468	0.007	100%		
		9/2	318841.8788	0.006	100%		
$2s^2 2p^4(^3\mathrm{P}_0)6f$	[3]°	7/2	319095.5118	0.003	100%		
		5/2	319095.8089	0.003	100%		
$2s^2 2p^4(^3\mathrm{P}_0)6g$	[4]	7/2	319111.6901	0.013	100%		
		9/2	319111.7080	0.007	100%		
$2s^2 2p^4(^3\mathrm{P}_0)6h$	[5]°		319114.94	0.02	100%		
$2s^2 2p^4(^3\mathrm{P}_2)7f$	[4]°	9/2	321405.23	0.02	100%		
		7/2	321405.91	0.06	91%	+ 9%	(^{3}P$_2$)7f[3]°
$2s^2 2p^4(^3\mathrm{P}_2)7f$	[3]°	7/2	321408.42	0.11	91%	+ 9%	(^{3}P$_2$)7f[4]°
		5/2	321408.60	0.07	99%		
$2s^2 2p^4(^3\mathrm{P}_2)7f$	[2]°	3/2	321420.46	0.14	100%		
		5/2	321420.66	0.06	99%		
$2s^2 2p^4(^3\mathrm{P}_2)7g$	[5]	9/2	321422.83	0.08	100%		
		11/2	321422.84	0.08	100%		
$2s^2 2p^4(^3\mathrm{P}_2)7g$	[4]	9/2	321423.21	0.08	100%		
		7/2	321423.22	0.08	100%		
$2s^2 2p^4(^3\mathrm{P}_2)7f$	[5]°	11/2	321423.96	0.08	100%		
		9/2	321423.99	0.07	100%		
$2s^2 2p^4(^3\mathrm{P}_2)7g$	[3]	5/2	321428.05	0.14	100%		
		7/2	321428.05	0.08	100%		
$2s^2 2p^4(^3\mathrm{P}_2)7g$	[6]	11/2	321431.02	0.11	100%		

Table 2. *Continued.*

Configuration	Term	J	Level (cm^{-1})	Uncert.[a] (cm^{-1})	Leading percentages[b]		
		13/2	321431.04	0.10	100%		
$2s^2 2p^4(^3P_2)7f$	[1]°	3/2	321433.97	0.10	100%		
$2s^2 2p^4(^3P_2)7g$	[2]	5/2	321434.54	0.14	100%		
$2s^2 2p^4(^3P_1)7f$	[2]°	3/2	322050.93	0.15	100%		
		5/2	322051.41	0.06	100%		
$2s^2 2p^4(^3P_1)7f$	[4]°	9/2	322055.98	0.02	100%		
		7/2	322056.39	0.04	100%		
$2s^2 2p^4(^3P_1)7g$	[3]	7/2	322066.84	0.08	100%		
		5/2	322066.86	0.08	100%		
$2s^2 2p^4(^3P_1)7g$	[5]	9/2	322068.50	0.08	100%		
		11/2	322068.56	0.08	100%		
$2s^2 2p^4(^3P_1)7f$	[3]°	7/2	322070.36	0.07	100%		
		5/2	322070.60	0.06	100%		
$2s^2 2p^4(^3P_1)7g$	[4]	7/2	322075.34	0.08	100%		
		9/2	322075.36	0.08	100%		
$2s^2 2p^4(^3P_0)7f$	[3]°	7/2	322337.35	0.05	100%		
		5/2	322337.87	0.09	100%		
$2s^2 2p^4(^3P_0)7g$	[4]	7/2	322348.00	0.08	100%		
		9/2	322348.00	0.08	100%		
$2s^2 2p^4(^3P_2)8f$	[4]°	9/2	323513.00	0.08	100%		
		7/2	323513.47	0.14	91%	+ 9%	$(^3P_2)8f[3]^\circ$
$2s^2 2p^4(^3P_2)8f$	[3]°	7/2	323515.12	0.12	91%	+ 9%	$(^3P_2)8f[4]^\circ$
$2s^2 2p^4(^3P_2)8f$	[2]°	5/2	323523.38	0.14	99%		
$2s^2 2p^4(^3P_2)8f$	[5]°	11/2	323525.49	0.09	100%		
		9/2	323525.51	0.09	100%		
$2s^2 2p^4(^3P_1)8f$	[2]°	3/2	324157.4	0.2	100%		
		5/2	324157.56	0.12	100%		
$2s^2 2p^4(^3P_1)8f$	[4]°	9/2	324160.95	0.09	100%		
		7/2	324161.30	0.09	99%		
$2s^2 2p^4(^3P_1)8f$	[3]°	7/2	324170.79	0.09	100%		
		5/2	324170.97	0.08	100%		
$2s^2 2p^4(^3P_0)8f$	[3]°	7/2	324441.04	0.08	100%		
		5/2	324441.18	0.08	100%		
$2s^2 2p^4(^3P_2)9f$	[4]°	9/2	324957.5	0.2			
$2s^2 2p^4(^3P_2)9f$	[5]°	9/2	324966.1	0.2			
		11/2	324966.1	0.2			
$2s^2 2p^4(^3P_1)9f$	[4]°	9/2	325603.7	0.2			
		7/2	325603.9	0.2			

Table 2. *Continued.*

Configuration	Term	J	Level (cm^{-1})	Uncert.[a] (cm^{-1})	Leading percentages[b]		
$2s^2 2p^4(^3\mathrm{P}_1)9f$	$[3]^\circ$	7/2	325610.5	0.2			
$2s^2 2p^4(^3\mathrm{P}_0)9f$	$[3]^\circ$	7/2	325882.8	0.2			
$2s^2 2p^4(^1\mathrm{D})4d$	^{2}G	9/2	327774.44	0.03	100%		
		7/2	327775.07	0.03	100%		
$2s^2 2p^4(^1\mathrm{D})4d$	^{2}F	5/2	328317.93	0.03	100%		
		7/2	328318.11	0.03	100%		
$2s^2 2p^4(^1\mathrm{D}_2)4f$	$[1]^\circ$	3/2	328568.864	0.014	100%		
		1/2	328568.87	0.03	100%		
$2s^2 2p^4(^1\mathrm{D}_2)4f$	$[5]^\circ$	9/2	328665.31	0.03	100%		
		11/2	328665.44	0.03	100%		
$2s^2 2p^4(^1\mathrm{D}_2)4f$	$[2]^\circ$	5/2	328695.864	0.015	100%		
		3/2	328695.882	0.015	100%		
$2s^2 2p^4(^1\mathrm{D}_2)4f$	$[3]^\circ$	5/2	328818.048	0.02	100%		
		7/2	328818.054	0.02	100%		
$2s^2 2p^4(^1\mathrm{D}_2)4f$	$[4]^\circ$	7/2	328847.027	0.02	100%		
		9/2	328847.124	0.02	100%		
$2s^2 2p^4(^1\mathrm{D})5s$	^{2}D	5/2	329148.63	0.04	98%		
		3/2	329148.77	0.04	98%		
$2s^2 2p^4(^1\mathrm{D}_2)5f$	$[1]^\circ$	3/2	338550.49	0.08	100%		
$2s^2 2p^4(^1\mathrm{D}_2)5f$	$[5]^\circ$	9/2	338600.85	0.12	100%		
		11/2	338600.86	0.12	100%		
$2s^2 2p^4(^1\mathrm{D}_2)5f$	$[3]^\circ$	5/2	338678.55	0.08	100%		
$2s^2 2p^4(^1\mathrm{D}_2)5f$	$[4]^\circ$	9/2	338693.67	0.10	100%		
		7/2	338693.73	0.10	100%		
$2s^2 2p^4(^1\mathrm{S})4s$	^{2}S	1/2	338788.75	0.09	58%	+ 40%	$(^1\mathrm{D})5d\,^2\mathrm{S}$
$2s^2 2p^4(^1\mathrm{D}_2)6f$	$[5]^\circ$	11/2	343994.03	0.2	100%		
		9/2	343994.03	0.2	100%		
$2s^2 2p^4(^1\mathrm{D}_2)6f$	$[4]^\circ$	9/2	344047.9	0.3	100%		
$2s^2 2p^4(^1\mathrm{D}_2)7f$	$[5]^\circ$	9/2	347244.1	0.2	100%		
		11/2	347244.1	0.2	100%		
$2s^2 2p^4(^1\mathrm{D}_2)8f$	$[5]^\circ$	11/2	349352.4	0.2	100%		

[a] The uncertainty of the $2s^2 2p^5\,^2\mathrm{P}^\circ_{1/2}$ level relative to the ground state (0.002 cm^{-1}) is due to the precise measurement of the forbidden $J = 3/2 - 1/2$ transition within the ground term [20]. The uncertainty of the $2s2p^6\,^2\mathrm{S}_{1/2}$ level is given relative to the ground state. The uncertainty of the $2s^2 2p^4(^3\mathrm{P})3s\,^4\mathrm{P}_{3/2}$ level is given relative to the $2s2p^6\,^2\mathrm{S}_{1/2}$ level. The uncertainties of all other levels with the principal quantum number $n \geq 3$ are given relative to the $2s^2 2p^4(^3\mathrm{P})3s\,^4\mathrm{P}_{3/2}$ level (see text).

[b] In this column, the core shells $2s^2 2p^4$ are omitted from configuration designations for brevity.

Table 3. Comparison of the mean ratios of the deviations of the observed wave numbers from the Ritz wave numbers derived from the newly optimized levels to the measurement uncertainties.

Source[a]	Number of lines[b]	rms $\lvert\sigma_{\rm Ritz} - \sigma_{\rm obs}\rvert$ / $\sigma_{\rm obs\,unc.}$
This work	82	1.3
Persson [1]	904	0.5
Palmer and Engleman [3]	256	0.7
Quinet et al. [5]	370	0.6
Boyce [18]	5	0.5

[a]Reference to the source of the measured wavelengths.
[b]The lines that alone determine one of the levels involved in the transition were excluded from the statistics.

From the rigorous statistical considerations on which the code LOPT is based, it follows that, if the adopted uncertainties of the observed wavelengths represent a 1σ scatter of a set of statistically independent measurements, then, on average, the line deviations should be approximately equal to the measurement uncertainties. In this case, the values of the ratio in the last column of Table 3 should be close to 1.0. The actual values of this ratio indicate that the adopted wavelength-measurement uncertainties listed in Table 1 may represent somewhat greater than one standard deviation for the lines quoted from Persson [1], Quinet et al. [5], and Boyce [18].

The Ritz wavelengths of the lines in Table 1 are in good agreement with those derived by Persson from his energy levels [1]. In the very important region below 460 Å, the mean difference between our Ritz wavelengths and those given by Persson is $+7\times10^{-5}$ Å with a standard deviation of 6×10^{-5} Å. In the region 990 Å to 2000 Å, the mean difference is $+1.3\times10^{-4}$ Å with a standard deviation of 3.3×10^{-4} Å. These differences are within the uncertainties stated by Persson, which confirms the good quality of the Ritz standards suggested by Persson [1]. The uncertainties of our Ritz wavelengths in the VUV are slightly smaller than those of Persson [1] because of the improved accuracy of the connection between the $2s2p^6$ configuration and configurations with $n \geq 3$. The uncertainties of the Ritz wavelengths in Table 1 are $\pm9\times10^{-5}$ Å at 300 Å (vs. Persson's $\pm1\times10^{-4}$ Å), $\pm1.2\times10^{-4}$ Å at 360 Å (vs. Persson's $\pm2\times10^{-4}$ Å), and $\pm2\times10^{-4}$ Å at 460 Å (vs. Persson's $\pm3\times10^{-4}$ Å).

Due to the large number of precisely measured lines, the accuracy of the Ritz wavelengths above 2000 Å given in Table 1 is notably better than it was possible to achieve using the energy levels from Persson [1] and Quinet et al. [5]. About 750 lines between 2000 Å and 18000 Å have Ritz wavelengths that are certain to $\pm1.5\times10^{-4}$ Å or better. These Ritz wavelengths can be used as secondary wavelength standards, provided that the lines are well resolved.

7 Parametric fitting

While analyzing the level scheme of Ne II, Persson [1] relied on Hartree-Fock calculations done in single configuration approximation without account for the configuration interaction (CI). In several cases, the term labels were assigned by comparison with series of levels with the same orbital momentum of the outermost electron. Persson [1] mentioned that CI is significant for the highly excited configurations and even causes switching of the levels with $ns\ ^4{\rm P}_{5/2}$ and $(n-1)d\ ^4{\rm P}_{5/2}$ as leading percentages between $n=5$ and $n=6$. Luyken [9] made a least-squares parametric fit of the $2p^43s$ and $2p^43d$ configurations and found the percentage composition of the eigenvectors. As a result of his fit, the $2p^4(^3{\rm P})3d\ ^4{\rm F}_{7/2}$ and $^2{\rm F}_{7/2}$ levels switched places as compared to the ab initio Hartree-Fock calculations. In his calculations, Luyken used effective parameters α and β to compensate for the combined effect of interactions with highly-lying configurations that were not included in the fit. The use of these parameters results in additions to the diagonal elements of the energy matrix. These additions are proportional to $\alpha L(L+1)$ and $\beta{\rm S}(S+1)$. Discussing Luyken's results, Persson [1] commented that these effective parameters were not well-defined for the $2p^43d$ configuration and, therefore, such calculations did not give enough reasons for changing the level names. Hartree-Fock calculations of Hansen and Persson [23], also accounting for the CI, produced the same order of the $^2{\rm F}_{7/2}$ and $^4{\rm F}_{7/2}$ levels as predicted by Luyken [9]. However, Hansen and Persson [23] considered their result as unreliable due to a high sensitivity of the term percentages to the parameters. However, the recent calculations using multiconfiguration Hartree-Fock codes by Tachiev and Froese Fischer [10] and Godefroid and Hibbert [24] also confirmed Luyken's assignment of the $^2{\rm F}_{7/2}$ and $^4{\rm F}_{7/2}$ levels. Therefore, the question of naming these two levels is now resolved in favor of Luyken. Since at least these two level designations needed revision in Persson's tables [1], additional calculations were necessary in order to verify the other assignments.

We made a parametric fit of the Ne II energy levels by means of Cowan's codes [25]. In these calculations, we included the following sets of configurations:

1. $2s^22p^5$, $(2s^22p^4+2p^6)np$ ($n=3$ to 8), $(2s^22p^4+2p^6)nf$ ($n=4$ to 8), $(2s^22p^4+2p^6)nh$ ($n=6$ to 8);
2. $2s2p^6$, $(2s^22p^4+2p^6)ns$ ($n=3$ to 8), $(2s^22p^4+2p^6)nd$ ($n=3$ to 8), $(2s^22p^4+2p^6)ng$ ($n=5$ to 8), $(2s^22p^4+2p^6)ni$ ($n=7$, 8).

The initial calculations were made using the HFR option of Cowan's RCN code with scaling of the F^k and G^k electrostatic parameters, as well as the CI radial parameters, by a factor of 0.9. After that, the Slater parameters were adjusted in order to fit all experimentally known energy levels except for the $2p^49f$ configuration. As Luyken [9] did, we also used the effective parameters α to describe the energy levels of the $2p^4nl$ configurations. We did not use the β parameters, since Cowan's codes do not support their usage in the configurations considered. Our use of

the α parameters is different from the standard way used by Luyken. These parameters were originally introduced in order to compensate for the unaccounted configuration interactions, when the calculations are done in the single-configuration approximation. In our case, we have a number of configuration interactions explicitly accounted for in the first order of the perturbation theory. Thus, if the configuration interactions are described correctly, the resulting values of the α parameters should be close to zero. However, with the initial values of the CI parameters fixed at 0.9 times the Hartree-Fock values, we obtained the best fit to the energy levels with negative values of the α parameters of about –400 cm^{-1}. This means that Cowan's Hartree-Fock code RCN overestimates the configuration interactions by a greater factor than the overestimation of the F^k and G^k parameters. When we reduced the CI parameters to approximately 0.7 of the Hartree-Fock values and made a new fitting, the values of the α parameters became very small, as expected. It should be noted that a slightly different result would be obtained if both the α and CI parameters were allowed to vary in the process of fitting. In this case, for unknown reason, a slightly better fitting of the energy levels is obtained with non-zero values of the α parameters. Thus, to obtain physically meaningful results, one should fix the CI parameters at smaller values than the ab initio ones and use the fitted values of α as an indicator of whether the values of the CI parameters were chosen properly. In the case of Ne II, strongly positive values of α indicate that the CIs are underestimated, while negative values indicate that the CIs are overestimated. This approach is in principle equivalent to fixing the α parameters to zero and allowing all the CI parameters linked together to vary. However, in the case of a large number of configurations, the latter procedure requires very large array dimensions because of the large number of the CI parameters. It is very hard to implement due to computer memory limitations.

The quality of our fitting can be characterized by the following: 190 odd levels were fit with 17 parameters with a standard deviation of 65 cm^{-1}, while 156 even levels were fit with 19 parameters with a standard deviation of 45 cm^{-1}. The detailed description of the parameters can be obtained from the authors. In order to save space, we only give the two leading percentages in the eigenvector composition, if they are greater than 5%.

The problem of assigning the $2p^4(^3\mathrm{P})3d\ ^4\mathrm{F}_{7/2}$ and $^2\mathrm{F}_{7/2}$ names to experimental levels indeed proved to be very subtle. The initial Hartree-Fock calculations place the $^4\mathrm{F}_{7/2}$ level below $^2\mathrm{F}_{7/2}$, as it was found by Persson [1]. The same level order results from the parametric fitting with the CI parameters fixed at 0.9 of their Hartree-Fock values. However, the final fitting with the CI parameters fixed at 0.7 of their Hartree-Fock values produces results that are in agreement with other calculations [9,10,23,24]. The same switching of the $^2\mathrm{F}_{7/2}$ and $^4\mathrm{F}_{7/2}$ levels occurs in our calculations for the other nd configurations ($n = 4$, 5, 6), with the purity of the lower $^2\mathrm{F}_{7/2}$ level increasing for higher values of n. The interchange of the $^2\mathrm{F}_{7/2}$ and $^4\mathrm{F}_{7/2}$ level names for the $2p^4(^3\mathrm{P})4d$ configuration was also pointed out by Hansen and Persson [23]. However, the interchange of the $2p^4(^3\mathrm{P})4d\ ^4\mathrm{P}_{5/2}$ and $^2\mathrm{F}_{5/2}$ level names, suggested by Hansen and Persson [23], was not confirmed by our calculations. Therefore, we retained original designations for these levels given by Persson [1].

In Table 2, we assigned the term labels to levels based on the maximum contribution of LS character. According to this principle, the $2p^4(^3\mathrm{P})ns\ ^4\mathrm{P}$ and $^2\mathrm{P}$ levels with $J = 3/2$ switch places between $n = 5$ and $n = 6$. The level names used by Persson [1] lead to a smooth behavior of the quantum defects along the series, but they are not consistent with the LS percentages. Based on the same principle of maximum LS percentage, we interchanged the level names of the $^4\mathrm{D}^\circ_{5/2}$ and $^2\mathrm{D}^\circ_{5/2}$ levels compared to Persson [1] in the $2p^4(^3\mathrm{P})5p$ and $6p$ configurations, as well as the $^4\mathrm{P}^\circ_{1/2}$ and $^2\mathrm{S}^\circ_{1/2}$ levels in the $6p$ configuration. Although, as mentioned by Persson [1], the LS labels have very little or no physical meaning for the highly mixed states, all our level-naming changes refer to the cases where the leading LS term accounts for more than 50% of the level character.

As noted by Persson [1], the levels with high angular momentum $l \geq 3$ are best described in the jK coupling scheme due to the almost negligible spin-orbit interaction of the outer electron.

Note added in proofs

Recently, Kramida et al. [26] investigated the VUV spectrum of Ne II between 286 Å and 325 Å with a Penning discharge in combination with the UV spectrum of the Pt/Ne lamp [7]. They revised identifications of two levels, $2p^4(^3\mathrm{P})7s\ ^2\mathrm{P}_{3/2}$ and $2p^4(^3\mathrm{P})6d\ ^4\mathrm{F}_{7/2}$ (in Tab. 2, they are at 318452.80 cm^{-1} and 318413.305 cm^{-1}, respectively). The new values of these levels are 318386.293 cm^{-1} and 318547.0 cm^{-1}, respectively [26]. According to these revisions, the identifications of the lines at 1449.132 Å, 1454.390 Å, 3708.449 Å [1], and 37270.24 Å [5] should be discarded from Table 1. As found in [26], effects of these revisions on the values of the other optimized levels, as well as Ritz wavelengths, is insignificant.

8 Conclusions

Having combined our FTS measurements with other published data, we have built a comprehensive list of approximately 1700 critically evaluated spectral lines of Ne II covering the region from 300 Å to 130000 Å. On the basis of this line list, we have derived an improved set of energy levels that is consistent with all observed lines. The accuracy of the previously used Ritz wavelengths in the VUV region suggested by Persson [1] has been notably improved. The improvement in accuracy is even greater for the Ritz wavelengths in the visible and infrared regions. The energy levels have been newly interpreted theoretically by means of Hartree-Fock calculations and parametric fitting, and this led to the revision of several level designations.

The authors are grateful to Dr. P. Quinet and Prof. E. Biémont for furnishing additional details about their measurements, to Prof. C. Froese Fischer for helpful discussions about theoretical calculations, and to Dr. C.J. Sansonetti for valuable suggestions and comments. This work was partly supported by the National Aeronautics and Space Administration and by the Office of Fusion Energy Sciences of the U.S. Department of Energy.

References

1. W. Persson, Phys. Scripta **3**, 133 (1971)
2. C.J. Sansonetti, M.M. Blackwell, E.B. Saloman, J. Res. Natl. Inst. Stand. Technol. **109**, 371 (2004)
3. B.A. Palmer, R. Engleman Jr, *Atlas of the Thorium Spectrum*, Los Alamos Natl. Lab. Report 9615, National Technical Information Service, Springfield, VA (1983)
4. E. Biémont, J.W. Brault, Phys. Scripta **34**, 751 (1986)
5. P. Quinet, P. Palmeri, E. Biémont, Phys. Scripta **49**, 436 (1994)
6. G. Nave, S. Johansson, A.P. Thorne, J. Opt. Soc. Am. B **14**, 1035 (1997)
7. J.E. Sansonetti, J. Reader, C.J. Sansonetti, N. Acquista, A.M. Sansonetti, R.A. Dragoset (2003), *Atlas of the Spectrum of a Platinum/Neon Hollow-Cathode Lamp in the Region 1130-4330 Å* (version 1.2); available: `http://physics.nist.gov/platinum` [2004, January 30]; Natl. Inst. Stand. Technol., Gaithersburg, MD
8. E.B. Saloman, C.J. Sansonetti, J. Phys. Chem. Ref. Data **33**, 1113 (2004)
9. B.F.J. Luyken, Physica **51**, 445 (1971)
10. G.I. Tachiev, C. Froese Fischer, Astron. Astrophys. **385**, 716 (2002); numerical results are available on the World Wide Web at `http://atoms.vuse.vanderbilt.edu/`
11. A.E. Kramida, G. Nave, Eur. J. Phys. D **37**, 1 (2006)
12. G. Norlén, Phys. Scripta **8**, 249 (1973)
13. W. Whaling, W.H.C. Anderson, M.T. Carle, J.W. Brault, H.A. Zarem, J. Quant. Spectrosc. Radiat. Transf. **53**, 1 (1995)
14. G. Nave, S. Johansson, R.C.M. Learner, A.P. Thorne, J.W. Brault, Astrophys. J. Suppl. Ser. **94**, 221 (1994); J. Sugar, C.H. Corliss, J. Phys. Chem. Ref. Data Suppl. **14**, 1 (1985); M. Rosberg, S.G. Johansson, Phys. Scripta **45**, 590 (1992); E. Biémont, S. Johansson, P. Palmeri, Phys. Scripta **55**, 559 (1997)
15. D. Zhechev, N. Parvanova, Opt. Commun. **212**, 301 (2002)
16. E.S. Chang, W.G. Schoenfeld, E. Bièmont, P. Quinet, P. Palmeri, Phys. Scripta **49**, 26 (1994)
17. J. Blaise, J.-F. Wyart, *Energy levels and atomic spectra of actinides*, Tables Int. Const. **20**, 1 (1992)
18. J.C. Boyce, Phys. Rev. **46**, 378 (1934)
19. B. Edlén, Int. J. Sci. Metrol. **2**, 71 (1966)
20. C. Yamada, H. Kanamori, E. Hirota, J. Chem. Phys. **83**, 552 (1985)
21. E.R. Peck, K. Reeder, J. Opt. Soc. Am. **62**, 958 (1972)
22. P. Quinet, private communication (1999)
23. J.E. Hansen, W. Persson, Phys. Scripta **8**, 197 (1973)
24. M.R. Godefroid, A. Hibbert, Mol. Phys. **98**, 1099 (2000)
25. R.D Cowan, The theory of atomic structure and spectra (University of California Press, Berkeley, 1981)
26. A.E. Kramida, C.M. Brown, U. Feldman, J. Reader, *Extended EUV and UV Spectrum of Ne II*, Phys. Scripta (2006, in press)